Computer Physics Communications ••• (••••) •••–•••

Contents lists available at ScienceDirect

Computer Physics Communications

www.elsevier.com/locate/cpc

Multiresolution scheme for Time-Dependent Schrödinger Equation

Emmanuel Lorin [a,c,*], A.D. Bandrauk [a,b]

[a] Centre de Recherches Mathématiques, Montréal, Québec, H3T 1J4, Canada
[b] Laboratoire de chimie théorique, Faculté des Sciences, Université de Sherbrooke, Québec, J1K 2R1, Canada
[c] School of Mathematics and Statistics, Carleton University, Ottawa, K1S 5B6, Canada

ARTICLE INFO

Article history:
Received 3 November 2009
Accepted 21 November 2009
Available online xxxx

Keywords:
Time-dependent Schrödinger equations
Finite difference methods
Mesh adaptation
Laser–molecule interactions

ABSTRACT

This paper is devoted to a multiresolution approach for solving laser–molecule Time-Dependent Schrödinger Equations (TDSE) in strong and high frequency fields. It is well known that short and intense laser–molecule interactions lead to complex nonlinear phenomena that necessitate an accurate numerical approximation of the TDSE. In particular, intense electric fields rapidly delocalize molecule wavefunctions so that their support can vary a lot during the interaction. In this kind of physical configurations, mesh adaption is a usual compromise between precision and computational efficiency. We then propose to explore numerically mesh adaptation for TDSE using a multiresolution analysis coupled with a Crank–Nicolson-like scheme. We then discuss the efficiency and the drawbacks of such a strategy.

1. Introduction

In this paper we explore mesh adaptation by multiresolution analysis for laser–molecule time-dependent Schrödinger equations (TDSE), that write:

$$\mathrm{i}\,\partial_t \psi(x,t) = \left[-\frac{1}{2}\partial_{xx} + V(x) + \theta(x)E(t)\right]\psi(x,t) \qquad (1)$$

where V is the Coulomb potential, $E \in C^2(\mathbb{R}_+)$ is the electric field, and ψ is the wavefunction. Function θ is equal to x on a bounded support and 0 otherwise. The role of this function is to limit the spatial influence of the electric field. We also assume that $|V|$ is bounded by V_∞, which is typically true for pseudo-potentials. Problem (1) is initialized with the ground state (first eigen-element) of the Hamiltonian operator $-\partial_{xx}/2+V$. This equation models quantum particles in an electric field, under the dipole approximation. The study of this equation is particularly crucial in the framework of *Attosecond Science* whose goal is to understand and control matter at the molecular scale [2]. The existence and regularity of this equation has been in particular, studied in [14].

For weak electric fields, a local refinement around the nuclei (under or beyond the Born–Oppenheimer approximation) is sufficient as the wavefunction remains localized around them. However, for strong electric fields it is well known (and easy to prove as very close to a classical electron motion) that the wavefunction is delocalized (with a global time-varying potential $V(x) + \theta(x)E(t)$), leading to several multiscale phenomena, such as the generation of high order harmonics and nonlinearities, above threshold ionization (ATI), *etc.* [4]. In order to simulate accurately these complex multiscale phenomena a very fine approximation is then necessary which justifies the use of an adaptive mesh method. The usual finite difference scheme used to approximate (1), is a Crank–Nicolson-like finite difference scheme with 3 or 5 point spatial stencils. Although it is very popular, from our knowledge, a stability study of this scheme on non-uniform meshes does not exist in the literature. We propose in this paper, its stability analysis. To limit the scheme overall computational complexity, we then propose to use a mesh adaption based on a multiresolution analysis. It is of course in the framework of image compression that wavelet and multiresolution techniques are the most used and successful. However, in the last 15 years many attempts have been proposed to use this tool for reducing the computational complexity of numerical methods for solving PDEs, hyperbolic and parabolic ones, in particular [11,7,9,6,10]. For time evolution problems, the general principle of a multiscale decomposition of the solution on a set of nested grids (from the coarsest to the finest one) and at each iteration. The solution is then redefined as the sum of functions defined on a coarse mesh, plus some details defined on the finer nested grids. Small details are then removed from the grids allowing a sparse representation of the solution, but keeping a good and controlled accuracy. In practice, at each iteration a new non-uniform mesh is built by MRA (justifying the study of analytical stability on non-uniform meshes) on which the solution is projected. For instance Figs. 1, 2 represent a ground state wavefunction ($R = 10$) on an adaptive mesh. From

* Corresponding author at: Centre de Recherches Mathématiques, Montréal, Québec, H3T 1J4, Canada.
E-mail address: lorin@crm.umontreal.ca (E. Lorin).

0010-4655/$ – see front matter
doi:10.1016/j.cpc.2009.11.012

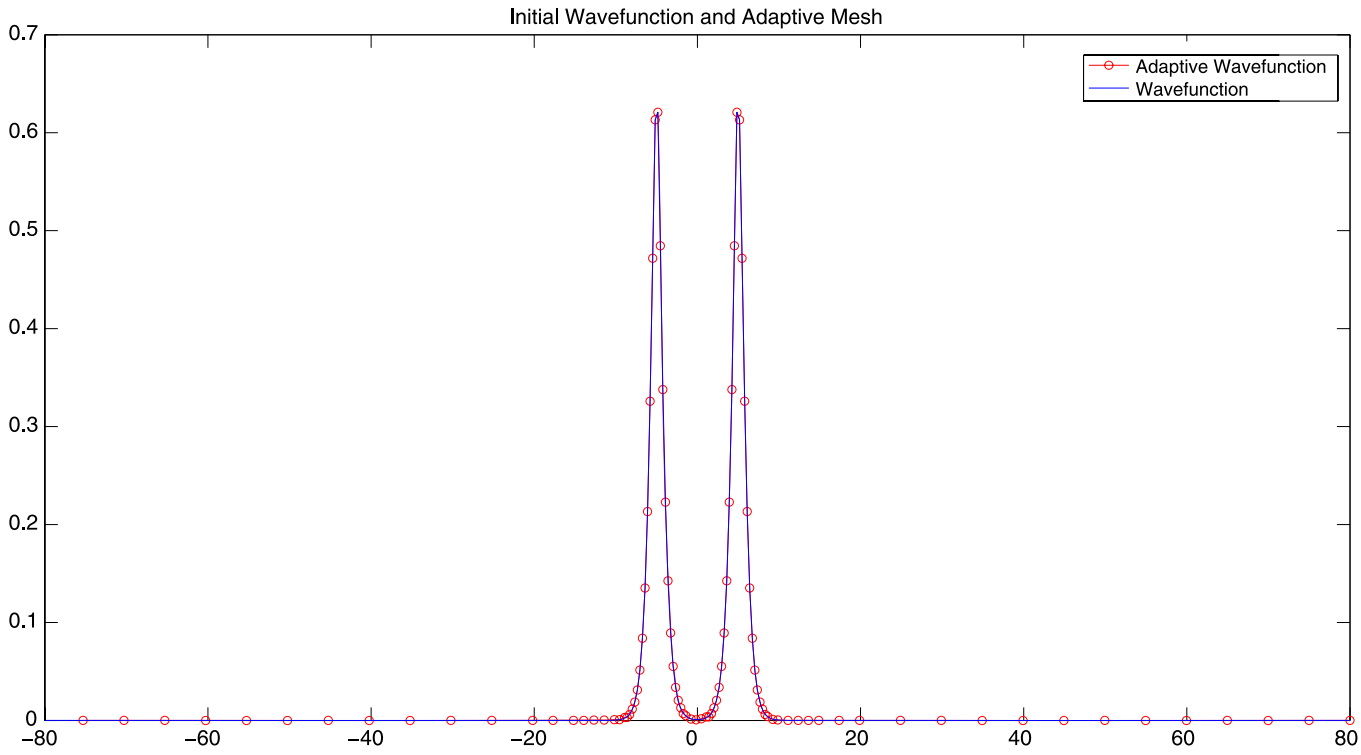

Fig. 1. Initial wavefunction, $R = 10$ for V defined by (8).

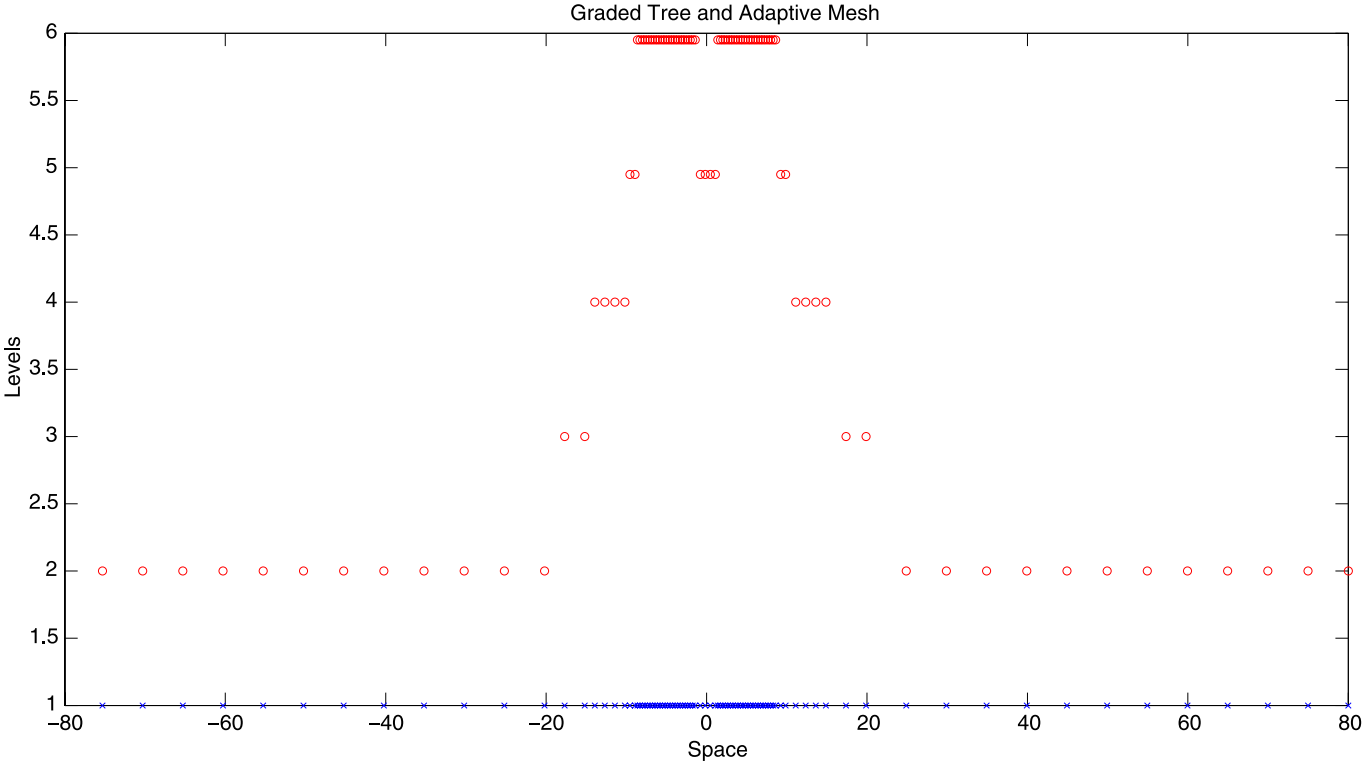

Fig. 2. Example of graded tree and adaptive mesh (5 levels).

another point of view, this decomposition consists of a representation of the solution on a multiscale basis (wavelets and scaling functions) where the small components are removed. The details of this decomposition will be recalled in Section 2. Note that in this paper, the choice of wavelets and scaling functions lead to a formulation that is very close to existing multigrid techniques. See in particular [5] or [1] for a deep comparisons between multiresolution and multigrid techniques. Although we consider in this paper a one-dimensional study, the principle of what follows can be extended in theory to higher dimensions, provided that Cartesian grids are used with efficient tensor product evaluation. Note that in the framework of TDSE numerical computation (time-independent

Please cite this article in press as: E. Lorin, A.D. Bandrauk, Multiresolution scheme for Time-Dependent Schrödinger Equation, Computer Physics Communications (2009), doi:10.1016/j.cpc.2009.11.012

and more recently time-dependent Schrödinger equations) a close approach (that have been shown to be very efficient) based on Discrete Variable Representation (DVR) bases have similarities with wavelet based methods. See [20] and [21] for details. The present work is also motivated by the fact that some complex models such as the Maxwell–Schrödinger model for laser–gas interaction and propagation presented in [14] require an accurate and very efficient computation of hundreds of thousands of one-dimensional TDSE. This communication is organized as follows. In Section 2, we present the chosen scheme for approximating the TDSE, we study its stability on non-uniform meshes. We then recall the basic notions of multiresolution analysis for mesh adaptation and we apply it to the quantum mechanics problem we consider. Section 3 is devoted to the numerical simulations, focusing on the gain in term of cell number reduction. We finally conclude in Section 4.

2. Scheme and analysis

We here recall the usual finite difference scheme that is used to approximate (1). It is a Crank–Nicolson-like scheme that writes on a non-uniform mesh, as follows

$$\begin{aligned}&\psi_j^{n+1}\big(1+a_j^{n+1}\big)+\psi_{j+1}^{n+1}b_j+\psi_{j-1}^{n+1}c_j\\&\quad=\psi_j^n\big(1+\bar a_j^n\big)+\psi_{j+1}^n\bar b_j+\psi_{j-1}^n\bar c_j\end{aligned}\tag{2}$$

where j is the space index, $\delta x_j = x_{j+1}-x_j$ are the space steps, n is the time index and

$$a_j^{n+1}=1-\mathrm{i}\frac{\delta t}{2}\big(V_j+\theta_j E^{n+1}\big)-\mathrm{i}\frac{\delta t}{4}\gamma_j,\qquad b_j=-\mathrm{i}\frac{\delta t}{4}\beta_j,$$
$$c_j=-\mathrm{i}\frac{\delta t}{4}\alpha_j$$

with

$$\alpha_j=\frac{2}{\delta x_{j-1}(\delta x_{j-1}+\delta x_j)},\qquad \beta_j=\frac{2}{\delta x_j(\delta x_{j-1}+\delta x_j)},$$
$$\gamma_j=\frac{2}{\delta x_j\delta x_{j-1}}.$$

We choose θ_j equal to x_j for $|j|\leqslant J$ and 0 otherwise, for some J in $\mathbb{N}^*$. Finally we assume (condition that will be ensured in the multiresolution process, *via* a graded tree) that $1/2\leqslant \delta x_{j-1}/\delta x_j\leqslant 2$ (in practice $\delta x_{j-1}/\delta x_j$ will belong to $\{1/2,2\}$). This scheme can obviously be written in the form

$$A^{n+1}\psi^{n+1}=B^n\psi^n\tag{3}$$

where A^{n+1} and B^n are two sparse matrices and $\psi^n=(\psi_i^n)_i$ is the approximate vectorial solution. In order to simplify the stability study, we will impose here Dirichlet's boundary conditions, on a sufficiently large computational domain (J large enough) in order to avoid or to reduce spurious reflexions. Details on more adapted boundary conditions can be found in [16].

Note now that another possible finite difference approach for solving (1) consists of taking

$$\begin{aligned}&\psi_j^{n+1}\big(1+a_j^n\big)+\psi_{j+1}^{n+1}b_j+\psi_{j-1}^{n+1}c_j\\&\quad=\psi_j^n\big(1+\bar a_j^n\big)+\psi_{j+1}^n\bar b_j+\psi_{j-1}^n\bar c_j,\end{aligned}\tag{4}$$

with

$$a_j^n=-\mathrm{i}\frac{\delta t}{2}\big(V_j+\theta_j E^n\big)-\mathrm{i}\frac{\delta t}{4}\gamma_j,\qquad b_j=-\mathrm{i}\frac{\delta t}{4}\beta_j,$$
$$c_j=-\mathrm{i}\frac{\delta t}{4}\alpha_j$$

so that we can rewrite (4)

$$\begin{aligned}&\psi_j^{n+1}\big(1+a_j^n\big)+\psi_{j+1}^{n+1}b_j+\psi_{j-1}^{n+1}c_j\\&\quad=\psi_j^n\big(1-a_j^n\big)-\psi_{j+1}^n b_j-\psi_{j-1}^n c_j.\end{aligned}\tag{5}$$

Note that spectral and finite element methods are also often used to solve (1) on complex geometries [3]. In the wavelet framework, choosing a finite volume/difference approach for solving (1), is equivalent to select particular scaling functions and mother wavelets. Inversely, any kind of scaling functions or wavelets could be selected to solve (1) using a Galerkin formulation with wavelet basis.

2.1. Stability

The scheme (2) (resp. (4)) is obviously stable when the spectral radius of $(A^{n+1})^{-1}B^n$ (resp. $(A^n)^{-1}B^n$) is less or equal to $1+K\delta t$, for some positive constant K. To determine a stability condition, rather than directly determining the spectral radius of $(A^{n+1})^{-1}B^n$ (resp. $(A^n)^{-1}B^n$), we use a discrete energy method and multiply by (2) by $\bar\psi_j^n(1+a_j^n)/2+\bar\psi_j^{n+1}(1-a_j^{n+1})/2$ (resp. $\bar\psi_j^n(1+a_j^n)/2+\bar\psi_j^{n+1}(1-a_j^n)/2$), and take the real part. Considering first (4), we obtain (skipping the details)

$$\begin{aligned}\big|\psi_j^{n+1}\big|^2=\big|\psi_j^n\big|^2&\\&-\frac{1}{1+|a_j^n|^2}\big[\mathrm{Im}\big(|b_j|\big(\psi_{j+1}^{n+1}+\psi_{j+1}^n\big)\big(1-a_j^n\big)\bar\psi_j^{n+1}\\&+|b_j|\big(\psi_{j+1}^{n+1}+\psi_{j+1}^n\big)\bar\psi_j^n\\&\times|c_j|\big(\psi_{j-1}^{n+1}+\psi_{j-1}^n\big)\big(1-a_j^n\big)\bar\psi_j^{n+1}\\&+|b_j|\big(\psi_{j-1}^{n+1}+\psi_{j-1}^n\big)\bar\psi_j^n\\&\times 2\big|a_j^n\big|^2\big(\psi_j^{n+1}\bar\psi_j^n+\psi_j^n\bar\psi_j^{n+1}\big)\big)\\&\times\mathrm{Re}\big(\big(1-\big|a_j^n\big|^2\big)\big(\psi_j^{n+1}\bar\psi_j^n-\psi_j^n\bar\psi_j^{n+1}\big)\\&-\big|a_j^n\big||b_j|\bar\psi_j^n\big(\psi_{j+1}^{n+1}+\psi_{j+1}^n\big)\\&+\big|a_j^n\big||b_j|\bar\psi_j^{n+1}\big(\psi_{j+1}^{n+1}+\psi_{j+1}^n\big)\\&+\big|a_j^n\big||c_j|\bar\psi_j^{n+1}\big(\psi_{j-1}^{n+1}+\psi_{j-1}^n\big)\\&-\big|a_j^n\big||c_j|\bar\psi_j^n\big(\psi_{j-1}^{n+1}+\psi_{j-1}^n\big)\big)\big].\end{aligned}$$

Now remark that $\mathrm{Im}(2|a_j^n|^2(\psi_j^{n+1}\bar\psi_j^n+\psi_j^n\bar\psi_j^{n+1}))=\mathrm{Re}((1-|a_j^n|^2)\times(\psi_j^{n+1}\bar\psi_j^n-\psi_j^n\bar\psi_j^{n+1}))=0$. We multiply by δx_j and sum over $j\in\mathbb{Z}$.

$$\begin{aligned}\sum_{j\in\mathbb{Z}}\delta x_j\big|\psi_j^{n+1}\big|^2=\sum_{j\in\mathbb{Z}}\delta x_j\big|\psi_j^n\big|^2-\sum_{j\in\mathbb{Z}}\delta x_j\frac{1}{1+|a_j^n|^2}&\\\times\big[\mathrm{Im}\big(|b_j|\big(\psi_{j+1}^{n+1}+\psi_{j+1}^n\big)\bar\psi_j^{n+1}&\\+|b_j|\big(\psi_{j+1}^{n+1}+\psi_{j+1}^n\big)\bar\psi_j^n&\\+|c_j|\big(\psi_{j-1}^{n+1}+\psi_{j-1}^n\big)\bar\psi_j^{n+1}&\\+|c_j|\big(\psi_{j-1}^{n+1}+\psi_{j-1}^n\big)\bar\psi_j^n\big)&\\\times\mathrm{Re}\big(\big|a_j^n\big||b_j|\big(\bar\psi_j^{n+1}\psi_{j+1}^{n+1}+\bar\psi_j^{n+1}\psi_{j+1}^n&\\-\bar\psi_j^n\psi_{j+1}^{n+1}+\bar\psi_j^n\psi_{j+1}^n\big)&\\+\big|a_j^n\big||c_j|\big(\bar\psi_j^{n+1}\psi_{j-1}^{n+1}+\bar\psi_j^{n+1}\psi_{j-1}^n&\\-\bar\psi_j^n\psi_{j-1}^{n+1}-\bar\psi_j^n\psi_{j-1}^n\big)\big)\big].&\end{aligned}$$

Remark 2.1. Note that when the mesh is uniform, that is $\delta x_j=\delta x$ for all j in $\mathbb{Z}$, we obtain from the previous equation the well-known equality

$$\|\psi^{n+1}\|^2_{\ell^2(\delta x\mathbb{Z})} = \sum_{j\in\mathbb{Z}} \delta x |\psi_j^{n+1}|^2 = \sum_{j\in\mathbb{Z}} \delta x |\psi_j^{n}|^2 = \|\psi^{n}\|^2_{\ell^2(\delta x\mathbb{Z})}.$$

That is the scheme is unconditionally ℓ^2-stable and non-dissipative (wavefunction conservation during the time evolution).

Going back to the general case, we remark that $|b_j| = |c_j|\frac{\alpha_j}{\beta_j} = |c_j|\frac{\delta x_j}{\delta x_{j-1}}$. We also denote by D_j the set of indices such that $\delta x_{j-1} \neq \delta x_j$ (corresponding to a change of spatial stepsize):

$$D_j = \{j \in \mathbb{Z},\ \delta x_j \neq \delta x_{j-1}\}.$$

It is then corresponded to the indices j such that $\delta x_j = r_{j-1}^j \delta x_{j-1}$ where r_{j-1}^j is the stepsize ratios with $r_{j-1}^j \in [1/2, 2]$ (this is an assumption that will be satisfied by our adapted meshes built by MRA). Then because of the cancellations similar to the uniform mesh case (see remark above), we have

$$\begin{aligned}
\sum_{j\in\mathbb{Z}} \delta x_j |\psi_j^{n+1}|^2 &= \sum_{j\in\mathbb{Z}} \delta x_j |\psi_j^{n}|^2 \\
&\quad - \sum_{jD_j} \frac{\delta x_j |b_j|}{1+|a_j^n|^2}\Bigg[\mathrm{Im}\Big((\psi_{j+1}^{n+1}+\psi_{j+1}^n)\bar\psi_j^{n+1} \\
&\quad + (\psi_{j+1}^{n+1}+\psi_{j+1}^n)\bar\psi_j^n \\
&\quad + \frac{\delta x_{j-1}}{\delta x_j}(\psi_{j-1}^{n+1}+\psi_{j-1}^n)\bar\psi_j^{n+1} \\
&\quad + \frac{\delta x_{j-1}}{\delta x_j}(\psi_{j-1}^{n+1}+\psi_{j-1}^n)\bar\psi_j^n\Big) \\
&\quad \times \mathrm{Re}\Big(|a_j^n|\big(\bar\psi_j^{n+1}\psi_{j+1}^{n+1} + \bar\psi_j^{n+1}\psi_{j+1}^n \\
&\quad - \bar\psi_j^n\psi_{j+1}^{n+1} - \bar\psi_j^n\psi_{j+1}^n\big) \\
&\quad + \frac{\delta x_{j-1}}{\delta x_j}\big(\bar\psi_j^{n+1}\psi_{j-1}^{n+1} + \bar\psi_j^{n+1}\psi_{j-1}^n \\
&\quad - \bar\psi_j^n\psi_{j-1}^{n+1} - \bar\psi_j^n\psi_{j-1}^n\big)\Big)\Bigg] \\
&= \sum_{j\in\mathbb{Z}} \delta x_j |\psi_j^{n}|^2 + \mathrm{LT}. \qquad (6)
\end{aligned}$$

This time we cannot *a priori* expect a cancellation of the last term of the rhs denoted by $\mathrm{LT} = \sum_{j\in D_j} \delta x_j \mathrm{LT}_j$. Note however that D_j has in practice a limited number of terms. Several important points have to be commented to address this issue. First, we easily see that when $|b_j| = \delta t/\delta x_j(\delta x_j + \delta x_{j-1})$ tends to zero (or more generally $\delta t/\delta x_o^2 \to 0$, with $\delta x_o = \min_{j\in\mathbb{Z}} \delta x_j$) the last term of (6) becomes negligible ensuring the stability of the scheme. Note also that for $|x_j|$ large enough and x_j close enough to the nucleus site, $|a_j^n|$ is very small. This allows to drop out additional terms in D_j. We then have

Proposition 2.1. *For $\delta t/\delta x_o^2$ small enough (2) is ℓ^2-stability (sufficient but not necessary condition): $\|\psi^{n+1}\|_{\ell^2(\delta x\mathbb{Z})} \leqslant (1 + K\delta t)\|\psi^n\|_{\ell^2(\delta x\mathbb{Z})}$ where K is a positive constant.*

However, such a condition ($\delta t/\delta x_o^2$ small enough) is very restrictive and can fortunately be lighten. Indeed, by writing (true by regularity) $\psi_{j+1}^n = \psi_j^n + \mathcal{O}(\delta x_j)$ we remark that

$$\begin{aligned}
\mathrm{LT}_j = -\frac{\delta x_j |b_j|}{1+|a_j^n|^2}\Bigg[&\mathrm{Im}\Big((\psi_{j+1}^{n+1}+\psi_{j+1}^n)\bar\psi_j^{n+1} \\
&+ (\psi_{j+1}^{n+1}+\psi_{j+1}^n)\bar\psi_j^n + \frac{\delta x_{j-1}}{\delta x_j}(\psi_{j-1}^{n+1}+\psi_{j-1}^n)\bar\psi_j^{n+1} \\
&+ \frac{\delta x_{j-1}}{\delta x_j}(\psi_{j-1}^{n+1}+\psi_{j-1}^n)\bar\psi_j^n\Big) \\
&\times \mathrm{Re}\Big(|a_j^n|\big(\bar\psi_j^{n+1}\psi_{j+1}^{n+1} + \bar\psi_j^{n+1}\psi_{j+1}^n - \bar\psi_j^n\psi_{j+1}^{n+1} - \bar\psi_j^n\psi_{j+1}^n\big) \\
&+ \frac{\delta x_{j-1}}{\delta x_j}\big(\bar\psi_j^{n+1}\psi_{j-1}^{n+1} + \bar\psi_j^{n+1}\psi_{j-1}^n - \bar\psi_j^n\psi_{j-1}^{n+1} \\
&- \bar\psi_j^n\psi_{j-1}^n\big)\Big)\Bigg].
\end{aligned}$$

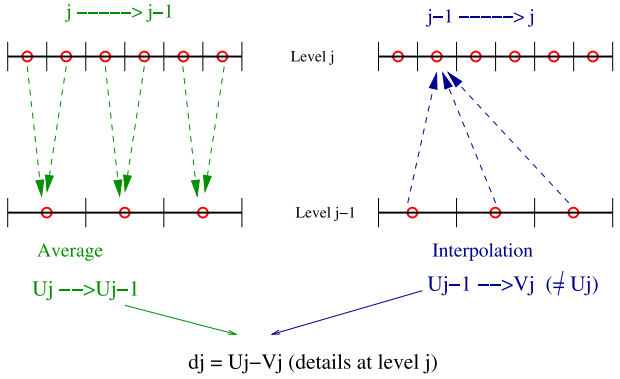

Fig. 3. Details.

Now it is easy to see that LT_j is negative up to $\mathcal{O}(\frac{\delta x_j|b_j|}{1+|a_j^n|^2})$ which then gives a *much less restrictive stability condition*, and much less numerical dissipation.

Similarly to (4) a stability study can be deduced for (2). This time, we multiply by $\bar\psi_j^n(1+a_j^n)/2 + \bar\psi_j^{n+1}(1-a_j^{n+1})/2$. We then deduce that $|\psi_j^{n+1}|^2 = \frac{1+|a_j^n|^2}{1+|a_j^{n+1}|^2}|\psi_j^n|^2 +$ additional terms. Now by definition of a_j^n, and noting that $E^{n+1} = E^n + \delta t(E')^n + \mathcal{O}(\delta t^2)$ we easily show that

$$|a_j^n| = \frac{|V_j + \theta_j E^{n+1} - \theta_j \delta t(E')^n + \mathcal{O}(\delta t^2)|}{2} + \frac{\delta t\gamma_j}{4}.$$

Now as $|(E')^n| \leqslant E'_\infty$, $|E^n| \leqslant E_\infty$, $|V_j| \leqslant V_\infty$ and $|\theta_j| \leqslant \theta_\infty$ we deduce that $|a_j^n| = |a_j^{n+1}| + \mathcal{O}(\delta t)$. The rest of the analysis is similar as above and then the result.

The scheme convergence can be deduced from the consistency and the Lax–Richtmyer equivalence theorem (see [18] for instance).

2.2. Multiresolution approach and mesh adaptation

We shortly recall the principle of the mesh adaptation using the multiresolution analysis. Details can be found in [11]. The goal of the paper is to study the feasibility and efficiency of multiresolution approaches in the framework of laser–molecule interaction in particular at high intensity and frequency. Note that the technique proposed in this paper corresponds to a coupling of several key approaches presented in [11,7,19,13].

First, we introduce a set of $L+1$ dyadic nested grids (from the finest L to the coarsest 0). We assume that the finest level (L) possesses N cells (power of 2) and the coarsest one $N/2^{L+1}$. Mesh adaptation using MRA can be summarized as follows. Start-

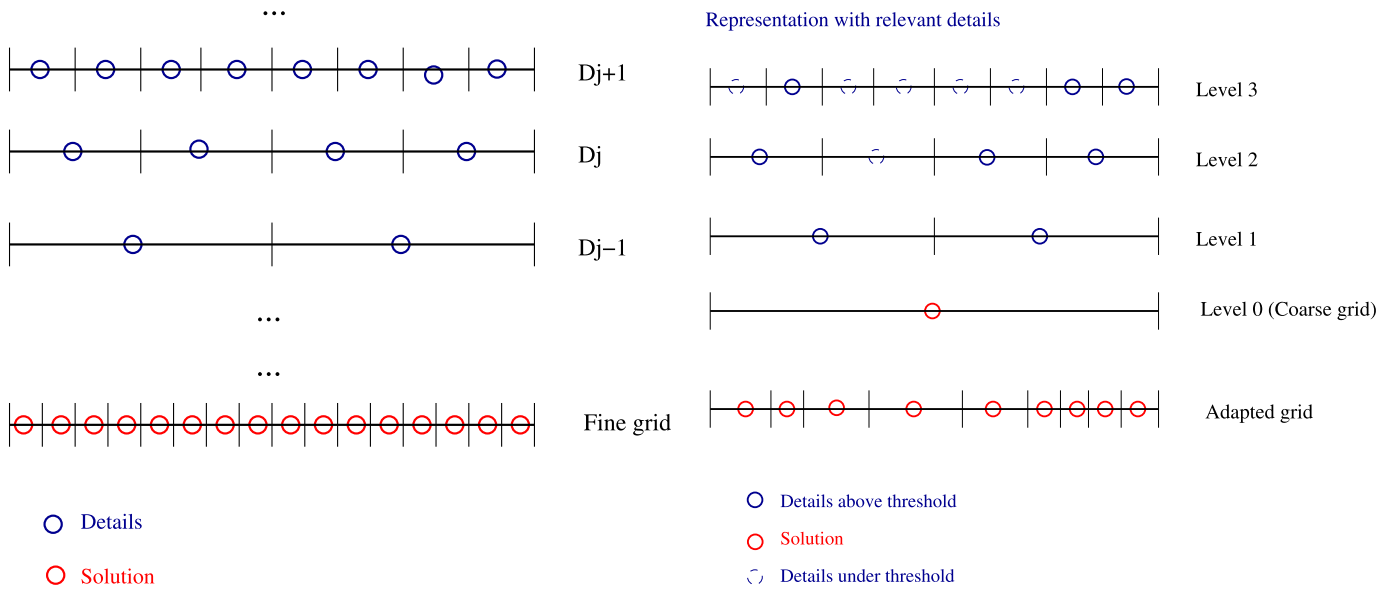

Fig. 4. Mesh adaptation.

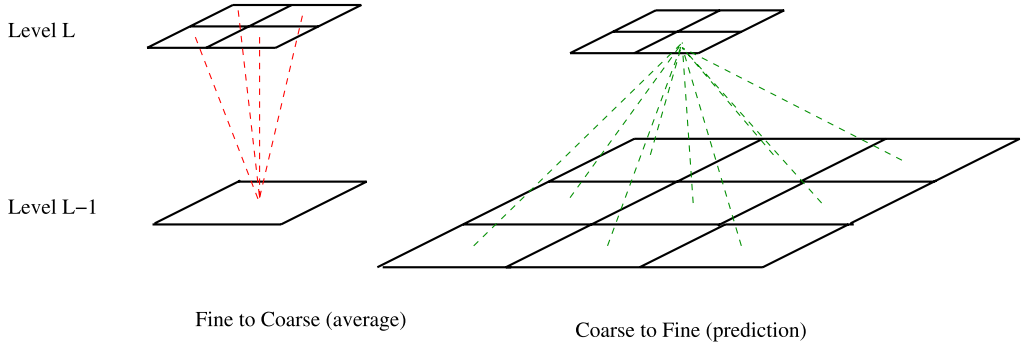

Fig. 5. *Fine to coarse* and *coarse to fine* processes.

ing from an initial data given on the finest mesh $\psi_L = (\psi_j)_j = (\int_{\Omega_j} \psi(x)\,dx/|\Omega_j|)_j$ (finite volume or P^0 formulation[1]), we have

- *Fine to coarse*. From level L to $L-1$, we define the wavefunction, on level $L-1$ ψ_{L-1}, by cell a simple cell *average* from the wavefunction ψ_L at level L, that is $\psi_{L-1,j} = (\psi_{L,2j} + \psi_{L,2j+1})/2$. This procedure is exact as the initial description is P^0.
- *Coarse to fine*. From level $L-1$ to L, we define $\hat{\psi}_L$ at the level L, by *polynomial interpolation* using ψ_{L-1}, that is $\hat{\psi}_{L,j} = \sum c_k \psi_{L-1,j\pm k}$ with some coefficients c_k. This interpolation is obviously exact only if $|\psi|$ is a polynomial of degree smaller or equal to the degree of approximation.
- *Details* are defined by $\mathbf{d}_L = (d_{L,j})_j := \psi_L - \hat{\psi}_L$ and consist of the error between the exact and predicted function (and then linked to the polynomial interpolation), at the Lth level.

By induction, we obtain a multiscale decomposition (where $\mathcal{M}$ is an encoding operator that requires $O(N)$ operations), Figs. 3, 4

$$\psi_L \Leftrightarrow (\psi_{L-1}, \mathbf{d}_L) \Leftrightarrow (\psi_{L-2}, \mathbf{d}_{L-1}, \mathbf{d}_L) \Leftrightarrow (\psi_0, \mathbf{d}_1, \ldots, \mathbf{d}_L) = \mathcal{M}\boldsymbol{\psi}_L.$$

We then have

- P^0-representation of ψ on the coarsest grid (level $\ell = 0$), denoted by ψ_0.
- $\mathbf{d}_1, \ldots, \mathbf{d}_L$ details from levels $\ell = 1$ to $\ell = L$.
- We finally get

$$\psi_L = (\psi_{L,j})_j = \sum_{\ell,j} d_{(\ell,j)} w_{(\ell,j)} + \sum_j \psi_{0,j} u_j \tag{7}$$

with ℓ level index and j space index,

where

- $\psi_{0,j} = (\psi, \tilde{u}_j)$ with $\tilde{u}_j = \mathbf{1}_{[jh,(j+1)h]}/h$ are the dual scaling functions.[2]
- $d_{(\ell',j')} = (\psi, \tilde{w}_{(\ell',j')})$: $\tilde{w}_{(\ell',j')} = \tilde{u}_{(\ell',j')} - \sum_{(\ell,j)} c_{(\ell,j,\ell',j')} \tilde{u}_{(\ell,j)}$ are the dual mother wavelets, where $\tilde{u}_{\ell,j}$ are the dual scaling functions at the intermediate levels ℓ, and given by $\mathbf{1}_{[2^{-\ell}jh, 2^{-\ell}(j+1)h]} h/2^\ell$. The expansion depends in particular on the order of polynomial interpolation.
- In practice for the programming approach, we do not use the formulation (7).

[1] Finite volume multiresolution is presented in [7] in the framework of hyperbolic systems of conservation laws.

[2] $\mathbf{1}_D(x)$ is equal to 1 if $x \in D$, 0 otherwise.

Please cite this article in press as: E. Lorin, A.D. Bandrauk, Multiresolution scheme for Time-Dependent Schrödinger Equation, Computer Physics Communications (2009), doi:10.1016/j.cpc.2009.11.012

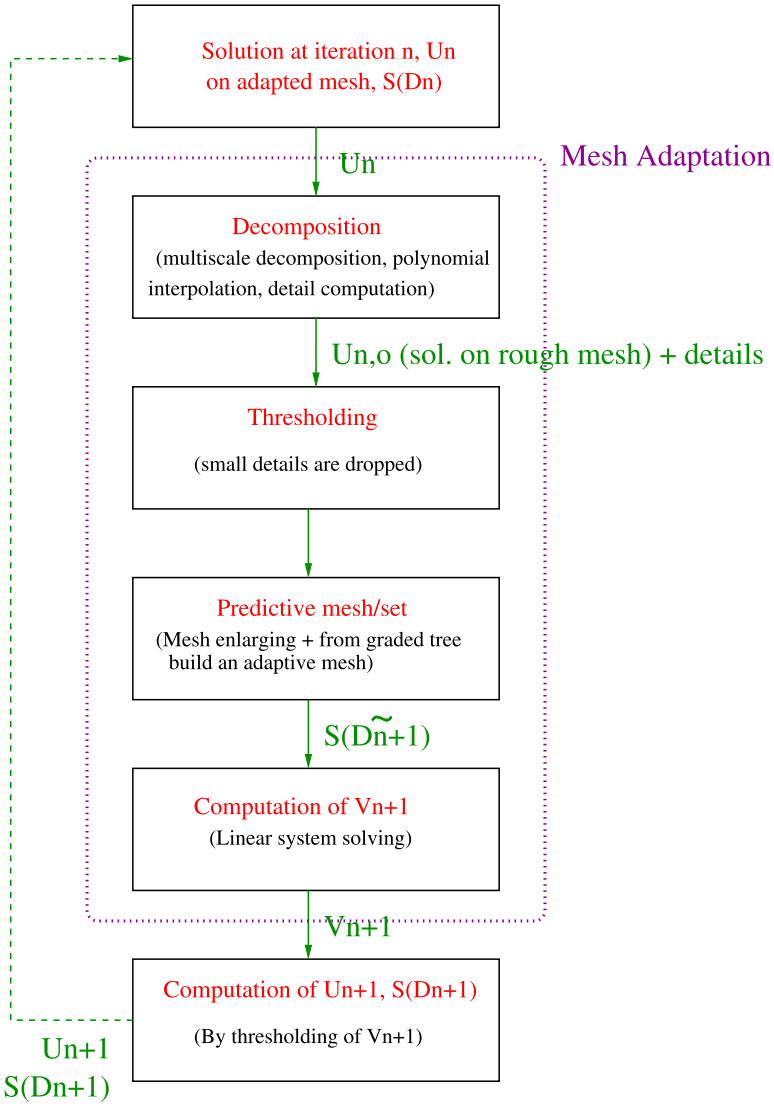

Fig. 6. Program structure.

Let us recall that in the MRA framework, where $(V_j)_j$ is a nested sequence (corresponding to the different discretization levels) satisfying the usual 6 MRA conditions, we have $L^2(\mathbb{R}) = \bigoplus_{j=-\infty}^{\infty} W_j$ where $V_L = V_0 \bigoplus_{j=0}^{L-1} W_j$ and V_j is spanned by $(u_{jk})_k = \{2^{j/2}u(2^j x - k),\ k \in \mathbb{Z}\}$ and W_j is spanned by $(w_{jk})_j = \{2^{j/2}w(2^j x - k),\ k \in \mathbb{Z}\}$. As a consequence any other choice of u, w would be possible (provided that they satisfy the usual MRA conditions and orthogonality properties). Then, the above multiscale decomposition corresponds to a special choice of scaling functions, and mother wavelets: the P^0 formulation imposes the scaling functions and the choice of the interpolation polynomials imposes the mother wavelets. Several key papers and books related to wavelets and their link with PDE solving exist, among them, let us cite [9,12] for hyperbolic PDEs. The next step is called thresholding and consists of canceling small details. More precisely details such that $|d_{(\ell,j)}| < \varepsilon_\ell$ with $(\mathbf{d}_\ell = (d_{\ell,j})_j)$ are dropped out, Fig. 4. This leads to a sparse representation $\boldsymbol{\Psi}_L$ of the function ψ_L on an *adaptive set* D (corresponding to the decomposition (7) dropping small details) of details or on an *adaptive mesh* $S(D)$ with rough discretization regions where details have been dropped. In other word the decomposition (7)

$$\boldsymbol{\Psi}_L = \sum_{(\ell,j)\in D^n} d_{(\ell,j)} w_{(\ell,j)} + \sum_j \psi_{0,j} u_j.$$

Now as is well known in wavelet theory (and proven in [7][3]) that the following inequality holds

$$\left|d_{(\ell,j)}\right| \leqslant \left(2^{-\ell}h\right)^s \|\psi\|_{C^s(\mathrm{supp}(2^{-\ell}jh, 2^{-\ell}(j+1)h))}.$$

For $\psi \in C^s$ and $s \leqslant n$ (order of accuracy of the prediction) we deduce that the adapted mesh will be *coarse* where ψ is *smooth*, which is all the interest of the mesh adaptation by MRA. In particular, this estimate allows to control exactly the error that is produced by dropping the small details. Note that this error has to be added to the error produced by the numerical scheme.

The prediction is a key step is the multiresolution approach and is detailed in [7,17]. This process will be repeated at each iteration.

2.3. Multiresolution scheme for TDSE

We now present the principle of the mesh adaptation for solving TDSEs. The general idea is then to reduce the number of cells having a fine description near large gradient regions and a coarse one near slowly varying regions. This then leads to reducing the

[3] The principle of the proof is based on 2 main arguments. The polynomial interpolation error combined with the fact that details are identically zero for polynomial of degree less or equal to the number of interpolation points minus 1.

Please cite this article in press as: E. Lorin, A.D. Bandrauk, Multiresolution scheme for Time-Dependent Schrödinger Equation, Computer Physics Communications (2009), doi:10.1016/j.cpc.2009.11.012

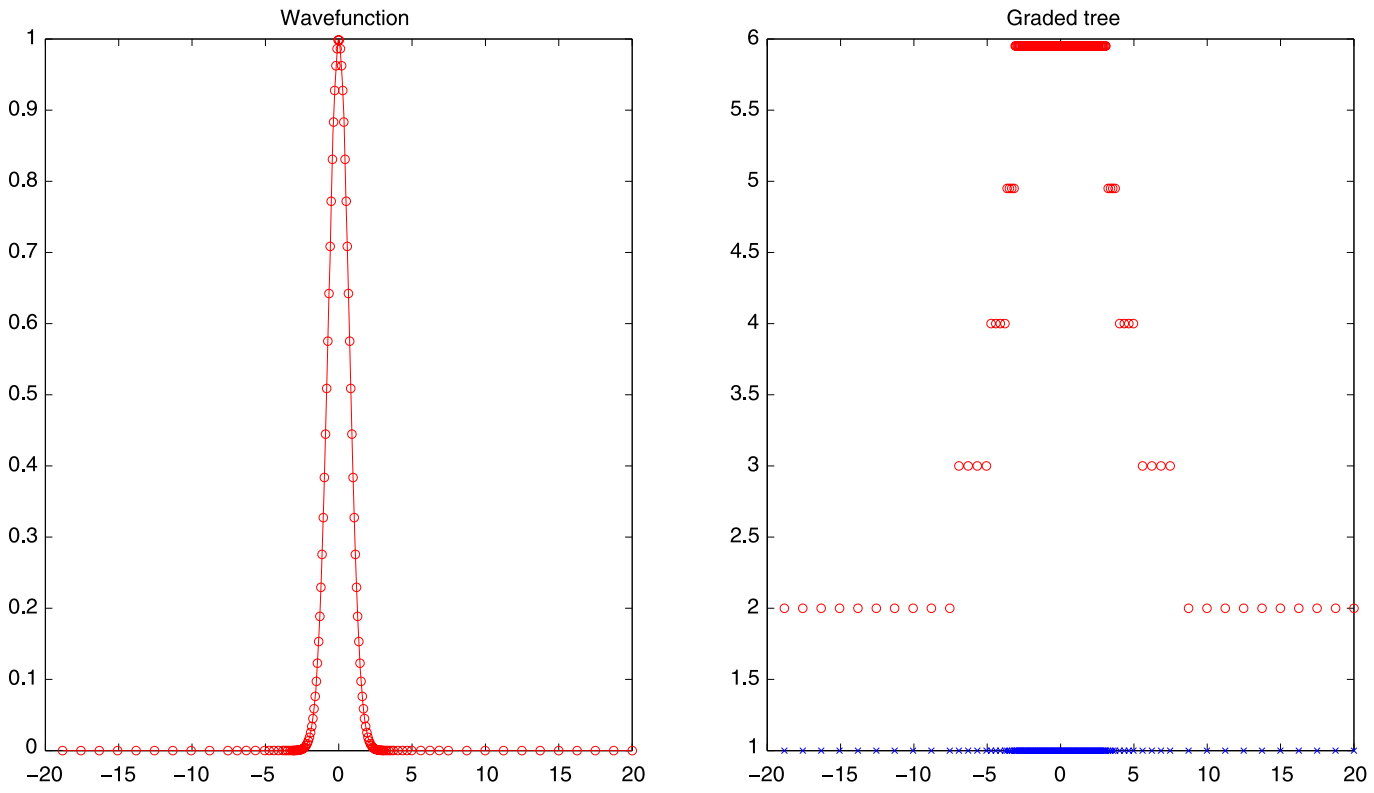

Fig. 7. Initial wavefunction, graded tree and adaptive mesh (5 levels), $T = 0$.

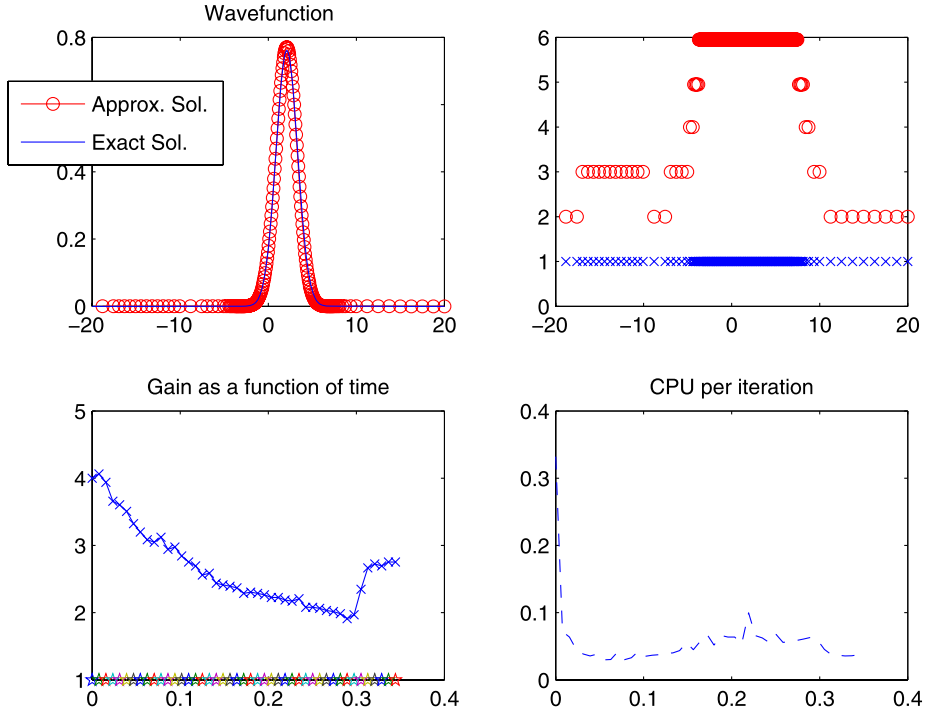

Fig. 8. Wavefunction, graded tree and adaptive mesh (5 levels), $T = t_1$.

size of the linear system (from Crank–Nicolson) to solve, but keeping a good and *controlled* accuracy. Note that, we do not apply the above multiresolution approach directly on the discrete wavefunction, but on its absolute value including the behavior of both the real and imaginary parts.

From ψ^n defined on the adapted mesh $S(D_N^n)$, we then apply the multiscale decomposition described above on $|\psi^n|$. By thresholding of the negligible details and enlarging, we obtain a predictive (using Cohen's approach [7] typically based on the detail magnitude[4]) adapted mesh $S(\tilde{D}_N^{n+1})$ (that contains $S(D^n)$ and $S(D^{n+1})$). We then update the solution on $S(\tilde{D}_N^{n+1})$ with δt^{n+1}

[4] Note that at a given level ℓ for a large detail d_k^ℓ, the associated cells $(2k, 2k+1)$ at the upper level $\ell+1$ are included in the predictive set. This corresponds to refine on the large detail regions also non-smooth regions of the wavefunction.

Please cite this article in press as: E. Lorin, A.D. Bandrauk, Multiresolution scheme for Time-Dependent Schrödinger Equation, Computer Physics Communications (2009), doi:10.1016/j.cpc.2009.11.012

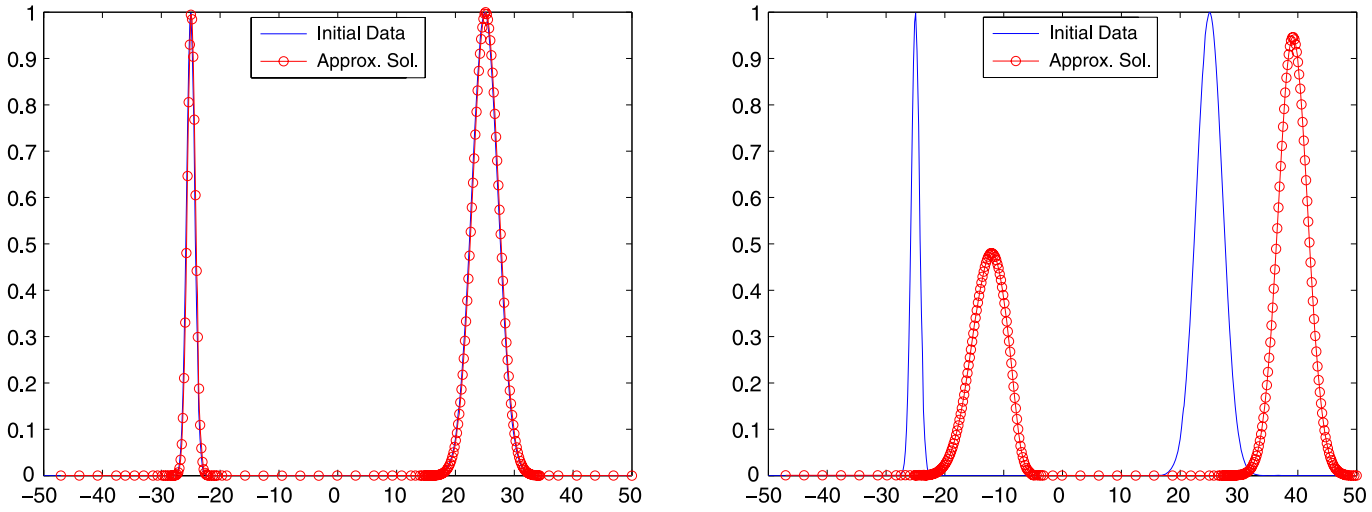

Fig. 9. Wavefunction and mesh motions for a wavepacket-like function.

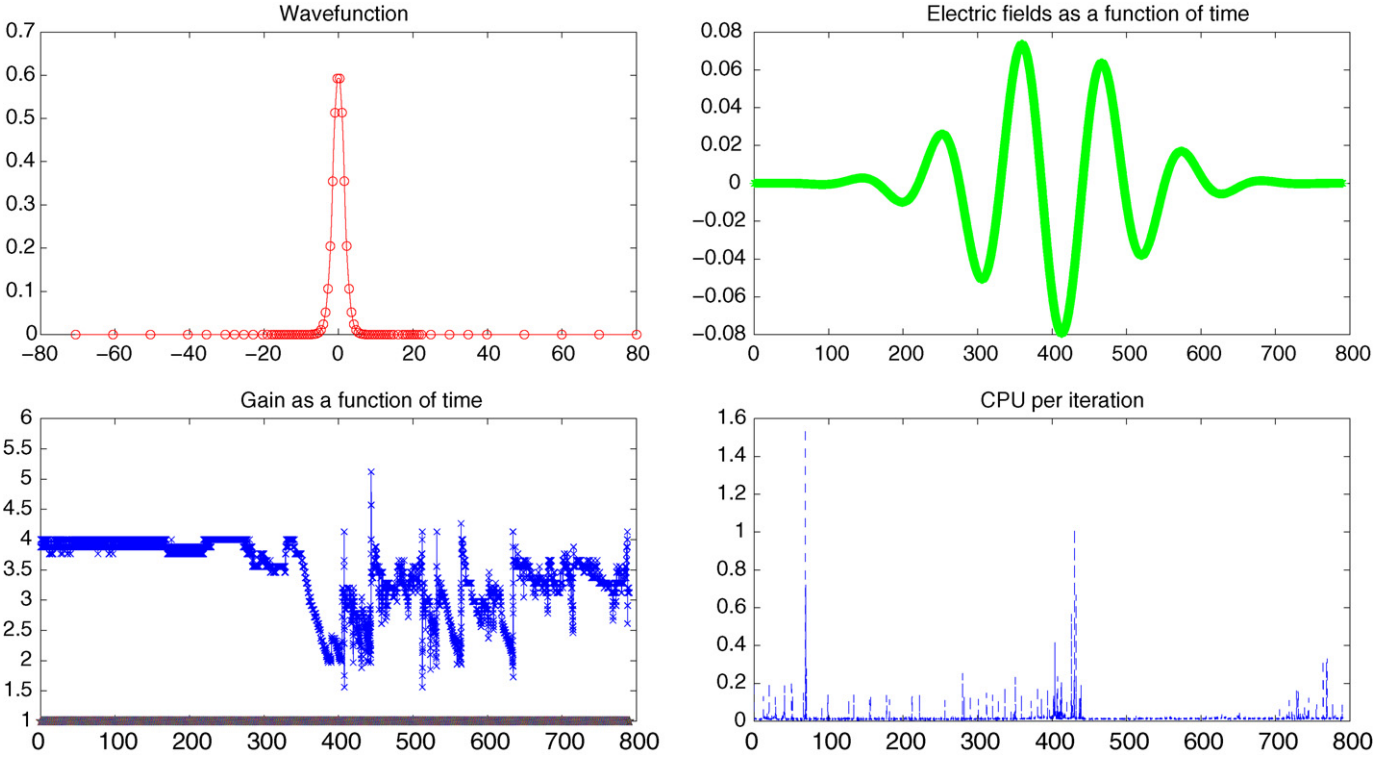

Fig. 10. Wavefunction – electric field/time – gain/time – CPU/iteration. $I = 0.08$.

satisfying the stability condition. We finally threshold again the solution $\tilde{\boldsymbol{\psi}}^{n+1}$ to obtain ψ^{n+1}. The procedure of multiscale decomposition, thresholding, recomposition is an $O(S(D_N^n))$ with in practice $S_N^n := \mathrm{Card}(S(D_N^n)) \ll N$ (see Fig. 6 and again [7] for details). Because of the sparse linear system solving (at each iteration) the complexity at iteration n, is only $O((S_N^n)^{3/2})$ rather than $O(N^{3/2})$ (typical computational complexity).

In order to have a better control of the gain G_N^n

$$G_N^n = \frac{N}{\#S_N^n}$$

we propose to add a constraint on $(\varepsilon_\ell)_\ell$. If the gain at iteration n is greater than a fixed $G_{\max}$, we divide by two each ε_ℓ (reduction of the threshold magnitude) allowing an increasing of the number of cells and a reduction of the gain. Inversely if the gain is less than $G_{\min}$, we multiply by 2 each ε_ℓ (increasing of the threshold magnitude) increasing the sparsity (but also the error) of the tree and then of the wavefunction representation.

The convergence and the error estimate can easily be deduced from Section 2.2. We denote by ψ_L the numerical solution on the finest level and by $\boldsymbol{\Psi}_L$ the solution on the adapted mesh obtained by multiscale decomposition, thresholding/enlarging and recomposition. Following the approach of [7], we deduce that for each iteration the error produced by the multiresolution algorithm (that will be added to the error produced by the finite difference/volume scheme), is as follows.

Proposition 2.2. *(See [7].) The compressed approximate wavefunction* $\boldsymbol{\Psi}_L^n$ *of* (1) *at time* t_n *satisfies*

Please cite this article in press as: E. Lorin, A.D. Bandrauk, Multiresolution scheme for Time-Dependent Schrödinger Equation, Computer Physics Communications (2009), doi:10.1016/j.cpc.2009.11.012

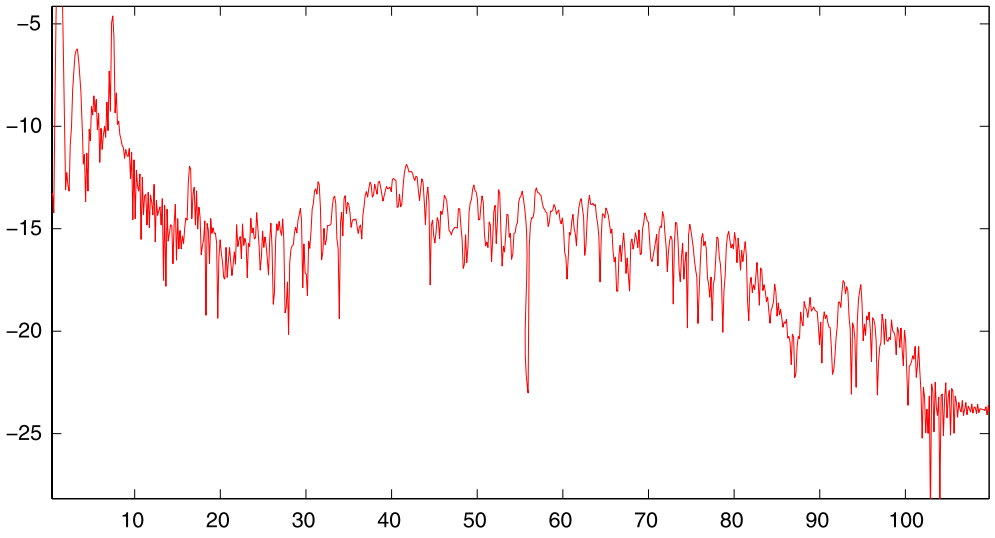

Fig. 11. Harmonic spectrum.

$$\left\|\psi_L^n - \boldsymbol{\Psi}_L^n\right\|_{\ell^1} \leqslant c \sum_{|d^n_{(\ell,j)}|<\varepsilon_\ell} |d^n_{(\ell,j)}| 2^{-\ell} h$$

where ψ_L^n is the approximate solution on the fine mesh.

Now at each iteration as we impose the time step to be such that the stability condition is satisfied, we deduce the convergence of the overall method.

2.4. Extension and improvement

We here discuss possible improvements and multidimensional extension of the method presented above.

In the following we denote by R_i the location of the m molecule nuclei ($i \in \{1, \ldots, m\}$) and by $B(R_i, r_i)$ an open ball centred in R_i of radius r_i. The union of these open balls is denoted by $\Omega_V = \bigcup_{i\in\{1,\ldots,m\}} B(R_i, r_i)$ and the global spatial domain is Ω. At anytime and for r_i small enough, the wavefunction will necessarily have large gradients in Ω_V (due Coulomb attractions). It is then useless to adapt the mesh in Ω_V that will be fine anyway. As a consequence, we apply the above mesh adaptation technique only on $\Omega - \Omega_V$ (adaptation process on $|\psi^n_{\Omega-\Omega_V}|$), that corresponds to the region where we can expect the largest gain in term of storage and CPU time reduction.

Additionally, for times t_n such that $|E(t_n)|$ is small enough, a mesh recalculation is not required. Indeed the wavefunction "motion" that is mainly driven by the electric field will vary slowly in time for low intensity fields. More generally the mesh recalculation period has to be inversely proportional to the electric field intensity.

Mesh adaptation by multiresolution analysis such as presented above is mainly still valid in higher dimension. In this framework scaling functions and wavelets simply consist of tensor products of the one-dimensional (in x, y, *etc.*) scaling functions and mother wavelets defined in this section. For instance, the natural extension of the *fine to coarse* (average) and *coarse to fine* (prediction/interpolation) processes is summarized in Fig. 5.

3. Numerical results

In this section, we present some numerical simulations illustrating the efficiency but also the limits of the presented approach. In particular, we focus on the gain in term of reduction of the number of cells and then of the size of linear systems to solve. Note that this gain is counter-balanced by a potentially restrictive stability constraints (see Section 2). The programming cost and flexibility of mesh adaptation by MRA, following the approach described above, is of main interest to make this method attractive for practical applications. Note first that the additional cost of programming is substantial but not prohibitive, and mainly consists of using different procedures that can be independently programmed (Fig. 6). The numerical data are as follows. The number of levels is 5 and $L = 4$. The number of cells at the finest level is $N = 2^m$. In our tests, we have chosen $m = 8, 9, 10$. The interpolation polynomials are chosen of degree 2, corresponding to take interpolation coefficients equal to $1, -1/8, 1/8$. The time steps have been chosen small enough to ensure stability.

A preliminary case is first proposed. The initial data is given by a Gaussian function $\psi_0(x) = \exp(\mathrm{i}k_0x)\exp(-x^2)$ on a domain $[-20, 20]$ with a wavenumber $k_0 = 3$. We assume that the electric field and Coulomb potential are zero and the factor $1/2$ in front of the Laplace operator in (1) was removed. In this case, the exact solution is given by

$$u(x,t) = \sqrt{\frac{\mathrm{i}}{\mathrm{i}-4t}}\exp\left(\frac{-\mathrm{i}x^2 - k_0x + k_0^2t}{\mathrm{i}-4t}\right).$$

We represent in Figs. 7, 8, the gain G_N^n as a function of time, the wavefunction modulus at two different times ($T = 0$ and $T = t_1$) and the corresponding graded tree ($m = 9$). Note that because of the increasing of the solution support the gain (reduction of the cell number) remains small in time ($G_N^n \sim 2$).

A second preliminary case, for an initial wavefunction that is the sum of two Gaussian functions is also proposed. We here just represent the solution at $t = 0$ and $t = 2$ with the corresponding mesh nodes (Fig. 9) showing the mesh motion during the time evolution. We consider now the interesting case: the laser–molecule interaction. The Coulomb potential we consider (corresponding to a H_2^+-molecule) is

$$V_c(R,x) = -\frac{1}{\sqrt{(x-R/2)^2+\eta}} - \frac{1}{\sqrt{(x+R/2)^2+\eta}} \tag{8}$$

with an internuclear distance denoted by R. The "regularization" parameter $\eta > 0$ is chosen such that the fundamental state is as close as possible to the physical one. Absorbing conditions are imposed [16] at the boundary of the domain $[-80, 80]$. The electric field is given by $E(t) = I\sin(\omega t)\exp(-5^{-5}(t-t_m)^2)$ with $I = 0.08$, $\omega = 0.056$ and $t_m = T_f/2 = 400$. This corresponds to a laser field

Please cite this article in press as: E. Lorin, A.D. Bandrauk, Multiresolution scheme for Time-Dependent Schrödinger Equation, Computer Physics Communications (2009), doi:10.1016/j.cpc.2009.11.012

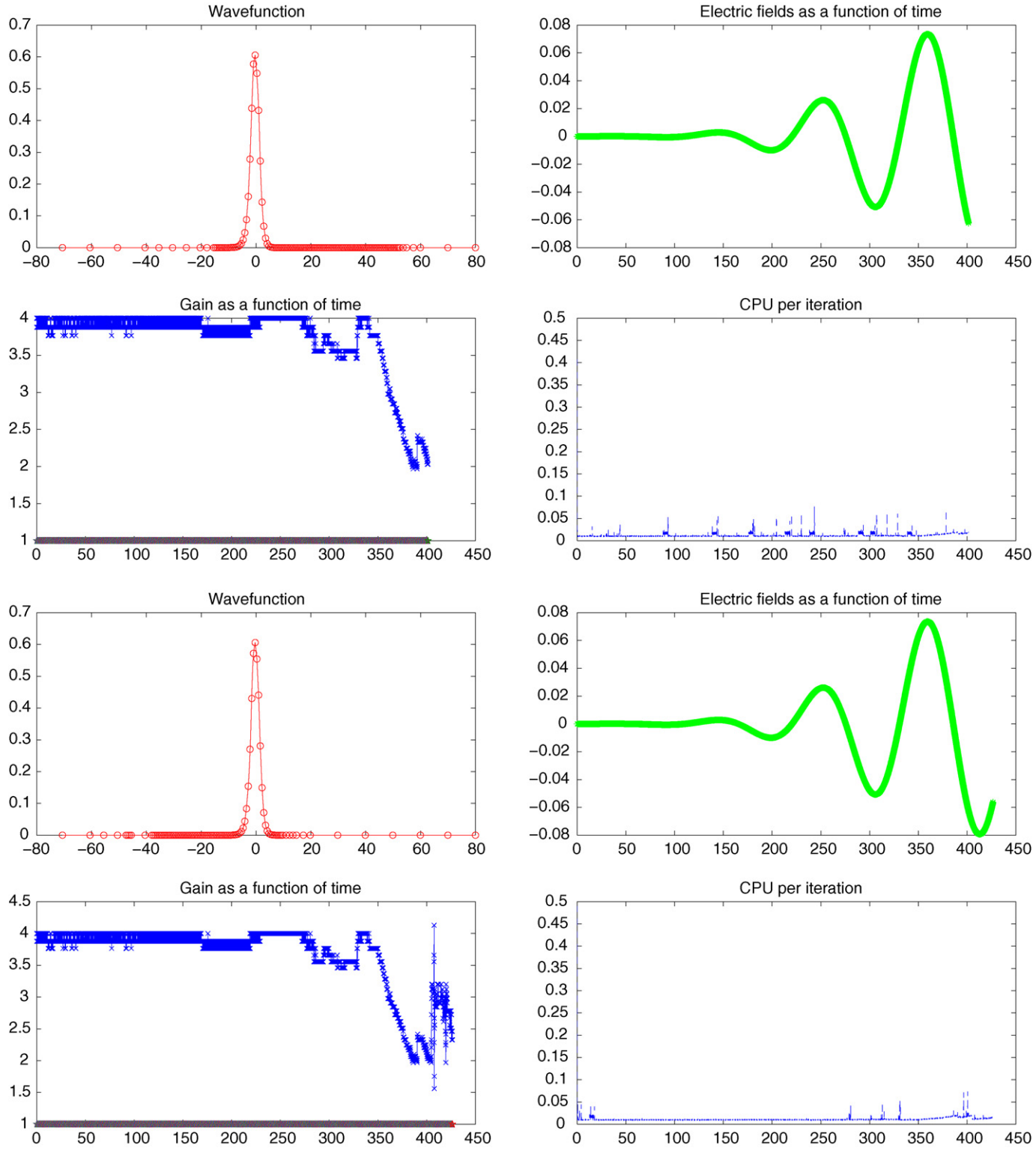

Fig. 12. Two intermediate times: Wavefunction – electric field/time – gain/time – CPU/iteration. $I = 0.08$.

of intensity 10^{14} W cm^{-2}, frequency 800 nm and duration of ~ 10 femtoseconds. From this set of physical data, we can expect high harmonic generation [8]. $\varepsilon_\ell = 2^{\ell-L}\varepsilon_L$ where ℓ is the level (from 0 to 4). As said in the introduction the initial data is determined by the first eigenpair of

$$-\left[\frac{1}{2}\partial_{xx} + V(x)\right]\psi_0(x) = \varepsilon_0\psi_0(x).$$

Numerical results are notably constituted by the absolute value of the solution (electron probability of presence), the Fourier transform of the harmonics spectrum (in logscale) of special interest in quantum chemistry and quantum optics (internal laser frequencies of a transmitted pulse, created by multi-photon ionization [8,14]).

$$p(t) = \int_{\mathbb{R}} x|\psi|^2(x,t)\,dx.$$

Please cite this article in press as: E. Lorin, A.D. Bandrauk, Multiresolution scheme for Time-Dependent Schrödinger Equation, Computer Physics Communications (2009), doi:10.1016/j.cpc.2009.11.012

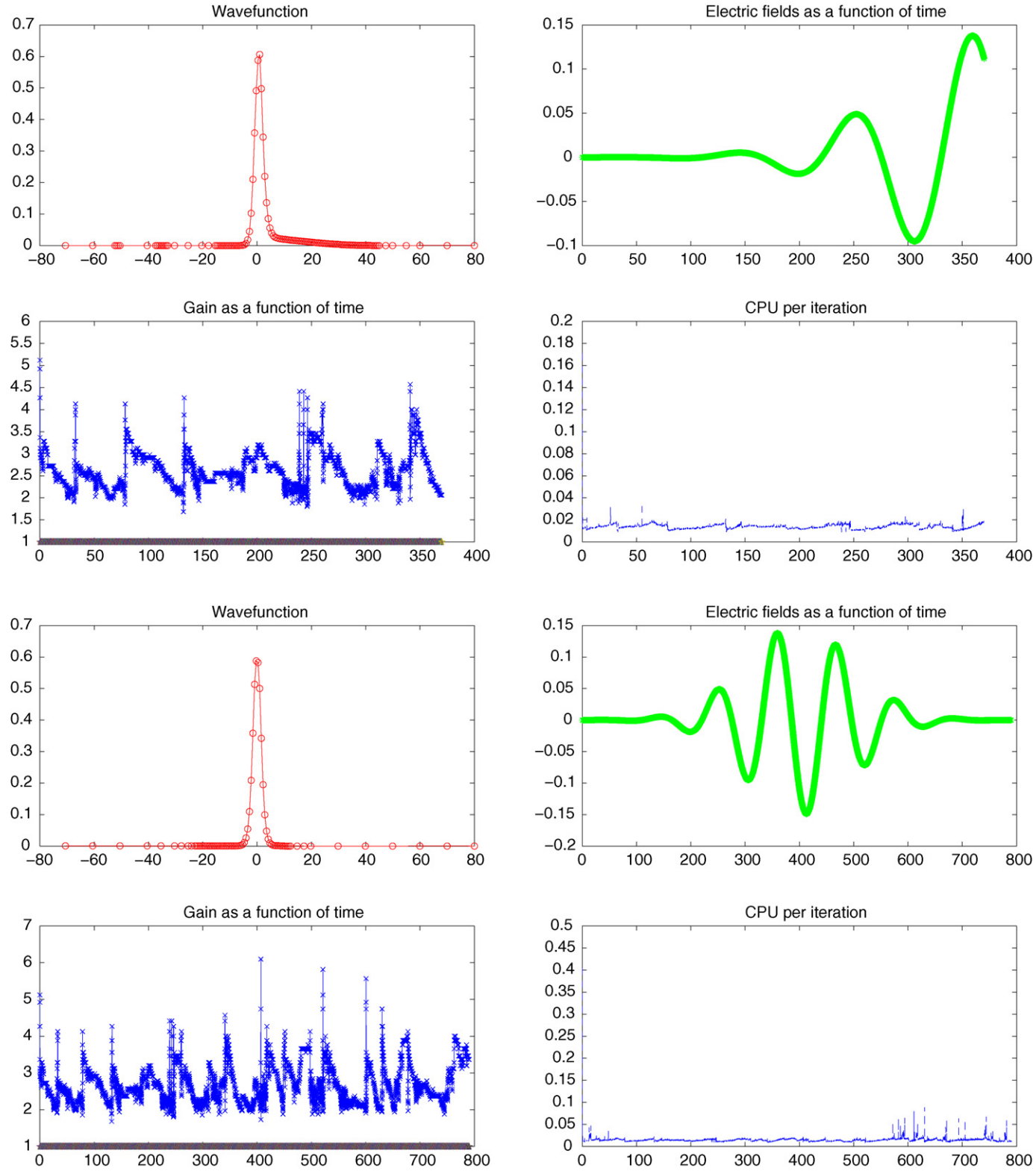

Fig. 13. Intermediate and final times: Wavefunction – electric field/time – gain/time – CPU/iteration. $I = 0.14$.

We also represent the mesh at different times and the corresponding wavefunction. Of main interest is the graph of the ratio G_N^n as a function of iterations n, that is the gain in term of cell reduction (ratio between the number of cells in the fine and adapted mesh). As the multiresolution process is of order S_N^n, the most time-consuming part is the resolution of the linear system (3). The effective gain is then of order G_N^α, $\alpha \sim 3/2$.

In the following, we choose $R = 2$, and make the scheme evolve in time. For a given tolerance (between "exact" and multiresolution solutions), we then represent in Fig. 10 with the data given above the electric field (right-top), the wavefunction (left-top) at time $t = T_f$ and the gain as a function of time (left-bottom). We observe that the gain varies between 2 and 5. Although the encoding-thresholding-predicting process is computational costly,

Please cite this article in press as: E. Lorin, A.D. Bandrauk, Multiresolution scheme for Time-Dependent Schrödinger Equation, Computer Physics Communications (2009), doi:10.1016/j.cpc.2009.11.012

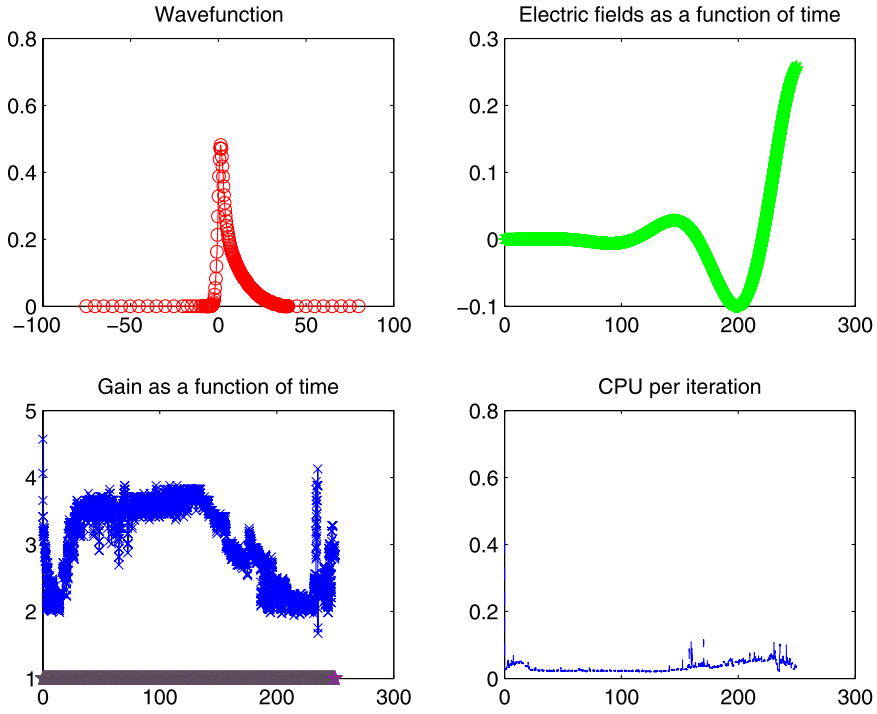

Fig. 14. First intermediate time: Wavefunction – electric field/time – gain/time – CPU/iteration. $I = 0.8$.

it is however an order S_N^n process with a large prefactor [7], so that for large N it is "negligible" compared to the solving of the linear system involved in the Crank–Nicolson-like scheme. This is why we have focused on the gain G_N^n, rather than the CPU time. However, graphs of CPU times are provided. Naturally an increasing of CPU time is observed when the corresponding gain curves are decreasing (for instance, Fig. 14). Note also that in the simulation (Fig. 10) we have applied the procedure described above on the increasing or decreasing of the threshold values. We finally represent the harmonic spectrum of the dipole moment showing the generation of high order harmonics in Fig. 11. Remark in particular that as expected for the H_2^+ molecule, the 7th harmonic is more intense than the 3rd one when $R = 2$ [15].

In the following figures (Fig. 12), we present the wavefunction modulus at 2 intermediate times. We observe that its support varies "a lot" during the interaction with the laser. This then justifies the use of a multiresolution approach.

We now increase the intensity of the laser pulse $I = 0.15$, and present similar results as above. As expected, the more intense the laser pulse is, the more delocalized the wavefunction will be requiring then an efficient mesh adaptation following the "motion of the electron". In this case, ε has been chosen equal to 10^{-4}, Fig. 13. To conclude we present at a given time a computed delocalized wavefunction with corresponding mesh and graded tree, to illustrate the moving adaptation. In this example, $I = 0.8$ and $N = 2^9$.

4. Conclusion

We have explored a fully adaptative multiresolution technique for solving TDSEs. The approach has shown to be efficient in reducing the total overall computational complexity of the scheme as well as maintaining a good accuracy (that is rigorously ensured by MRA). Moreover, a big flexibility in the mesh adaptation is provided by the choice of the threshold value. The main gain is *in fine* the reduction of the size of the sparse linear system arising from the Crank–Nicolson scheme. It is important to note however, that the non-uniformity of the mesh leads potentially to a loss of stability of the scheme, and then to imposing a restrictive constraint on the time step, that overall counter-balances the MRA mesh adaptation. However, in practice we do not observe a large discrepancy of the stability and then recommend the use of such a technique. The extension to higher dimension does not involve any additional theoretical difficulties, and is currently in progress.

References

[1] A. Avudainayagam, C. Vani, Wavelet based multigrid methods for linear and nonlinear elliptic partial differential equations, Appl. Math. Comput. 148 (2) (2004) 307–320.

[2] A. Bandrauk, S. Chelkowski, Attosecond science – the next frontier, La Physique au Canada 65 (1) (2009).

[3] A.D. Bandrauk, H.-Z. Lu, Numerical methods for molecular time-dependent Schrödinger equations – bridging the perturbative to nonperturbative regime, in: Handbook of Numerical Analysis, vol. X, North-Holland, Amsterdam, 2003, pp. 803–832.

[4] R.W. Boyd, Nonlinear Optics, 2nd edition, Academic Press, 2003.

[5] W.L. Briggs, V.E. Henson, Wavelets and multigrid, SIAM J. Sci. Comput. 14 (1993) 506–510.

[6] A. Cohen, Wavelet methods in numerical analysis, in: Handbook of Numerical Analysis, vol. VII, North-Holland, Amsterdam, 2000, pp. 417–711.

[7] A. Cohen, S.-M. Kaber, S. Müller, M. Postel, Fully adaptive multiresolution finite volume schemes for conservation laws, Math. Comp. 72 (241) (2003) 183–225 (electronic).

[8] P.-B. Corkum, Plasma perspective on strong-field multiphoton ionization, Phys. Rev. Lett. 71 (1993) 1994.

[9] W. Dahmen, Wavelet methods for PDEs – some recent developments, J. Comput. Appl. Math. 128 (1–2) (2001) 133–185, Numerical Analysis 2000, vol. VII, Partial Differential Equations.

[10] I. Daubechies, Ten Lectures on Wavelets, CBMS-NSF Regional Conference Series in Applied Mathematics, vol. 61, Society for Industrial and Applied Mathematics (SIAM), Philadelphia, PA, 1992.

[11] A. Harten, Adaptative multiresolution schemes for shock computations, J. Comput. Phys. 115 (1994) 319–338.

[12] M. Holmström, J. Waldén, Adaptive wavelet methods for hyperbolic PDEs, J. Sci. Comput. 13 (1) (1998) 19–49.

[13] N. Hovhannisyan, S. Müller, On the stability of fully adaptative multiscale schemes for conservation laws using approximate flux and source reconstruction strategies, 2009, submitted for publication.

Please cite this article in press as: E. Lorin, A.D. Bandrauk, Multiresolution scheme for Time-Dependent Schrödinger Equation, Computer Physics Communications (2009), doi:10.1016/j.cpc.2009.11.012

[14] E. Lorin, S. Chelkowski, A. Bandrauk, A numerical Maxwell–Schrödinger model for laser–matter interaction and propagation, Comput. Phys. Comm. 177 (12) (2007) 908–932.

[15] E. Lorin, S. Chelkowski, A. Bandrauk, Attosecond pulse generation from aligned molecules – dynamics and propagation in H_2^+, New J. Phys. 10 (2008), Art. ID 025033, 21 pp.

[16] E. Lorin, S. Chelkowski, A. Bandrauk, Mathematical modeling of boundary conditions for laser–molecule time dependent Schrödinger equations and some aspects of their numerical computation. One-dimensional case, Numer. Methods Partial Differential Equations 25 (1) (2009) 110–136.

[17] S. Müller, Y. Stiriba, A multilevel finite volume method with multiscale-based grid adaptation for steady compressible flows, J. Comput. Appl. Math. 227 (2) (2009) 223–233.

[18] A. Quarteroni, R. Sacco, F. Saleri, Numerical Mathematics, second edition, Texts in Applied Mathematics, vol. 37, Springer-Verlag, Berlin, 2007.

[19] O. Roussel, K. Schneider, A. Tsigulin, H. Bockhorn, A conservative fully adaptive multiresolution algorithm for parabolic PDEs, J. Comput. Phys. 188 (2) (2003) 493–523.

[20] B.I. Schneider, D.L. Feder, Numerical approach to the ground and excited states of the Bose–Einstein condensed gas confined in a completely anisotropic trap, Phys. Rev. A 59 (1999) 2232–2242.

[21] B.I. Schneider, D.L. Feder, The discrete variable method for the solution of the time dependent Schroödinger equation, J. Non-Cryst. Solids 351 (18) (2005) 1551–1558.

Please cite this article in press as: E. Lorin, A.D. Bandrauk, Multiresolution scheme for Time-Dependent Schrödinger Equation, Computer Physics Communications (2009), doi:10.1016/j.cpc.2009.11.012